

SUPPORTING INFORMATION for:

A new, superionic, plastic polymorph of the Na⁺ ion conductor Na₃PS₄

*Theodosios Famprakis**, James A. Dawson, François Fauth, Oliver Clemens, Emmanuelle Suard, Benoit Fleutot, Matthieu Courty, Jean-Noël Chotard, M. Saiful Islam* and Christian Masquelier*

Corresponding Authors

theo.famprakis@u-picardie.fr; m.s.islam@bath.ac.uk; christian.masquelier@u-picardie.fr

Synthesis

Na₃PS₄ was synthesized from the binaries Na₂S and P₂S₅ (Sigma-Aldrich) by a solid-state synthesis route^{1,2}. Stoichiometric ratios of the reagents were intimately mixed, pelletized and placed in carbon-coated quartz tubes. The carbon-coating of the tubes was achieved by acetone pyrolysis and subsequent annealing at 1000 °C for 12 h under Ar. The quartz tubes were then flame-sealed under vacuum (10⁻² mbar) and placed in a furnace for reaction. The temperature of the furnace was slowly increased to 500 °C at 1 °C/min, held for 20 h and naturally cooled to room temperature. The reacted pellets were then milled by pestle and mortar into a fine powder for further analysis. All handling was performed in Ar-filled gloveboxes.

Neutron powder diffraction

The crystallinity of Na₃PS₄ above 500 °C was first serendipitously observed during neutron diffraction experiments at the D2B beamline of the Institute Laue-Langevin in Grenoble, France. Na₃PS₄ samples were placed in 10-mm cylindrical vanadium containers under Ar, which were then put inside a vacuum furnace connected to a secondary pump. Diffractograms were collected through the vanadium walls and heating elements of the furnace in transmission geometry, using a 2-D array of ³He tube detectors and a wavelength of 1.594 Å, selected using the 335 reflection of a monocrystalline Ge monochromator.

Due to a user error, the temperature in the furnace was raised to 550 °C, presumably above the melting point, and it was surprisingly observed that the sample was exhibiting Bragg diffraction. Due to time and scope limitations, only a very short ~1.5 h preliminary measurement was taken at 510 °C, which is presented below, and further study was pursued by means of synchrotron x-ray diffraction.

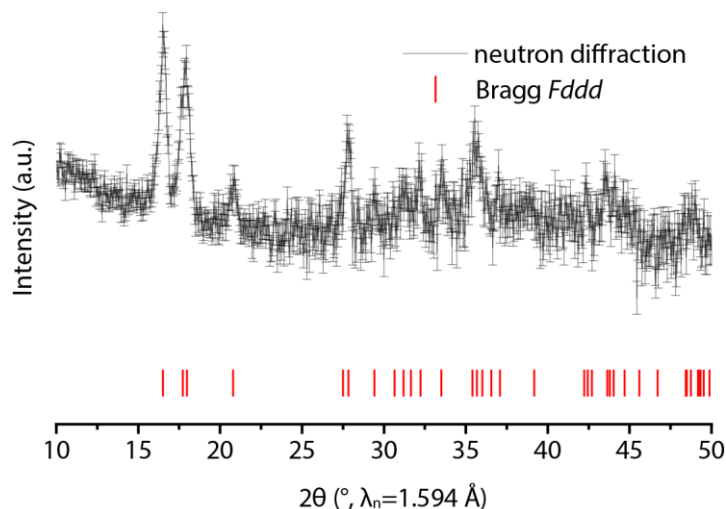


Figure S1. Preliminary neutron diffractogram of Na_3PS_4 exhibiting Bragg diffraction at 510 °C

Synchrotron x-ray powder diffraction

X-ray diffraction experiments were performed at the MSPD beamline^{3,4} of the ALBA synchrotron in Barcelona, Spain. Samples were flame-sealed under Ar in 1-mm-diameter quartz capillaries and the temperature was controlled using a hot air blower. Diffractograms were collected in transmission geometry, using a position-sensitive MYTHEN detector and a wavelength of 0.8264 Å, selected using a Si 111 reflection double crystal monochromator. Short measurements (30 s) were continuously recorded on heating and cooling from room temperature to 550 °C and back, at a rate of 5 °/min. A longer measurement (270 s) was taken at 550 °C for refinement;

Analysis of diffraction data

Analysis of the diffraction data was performed using various programs in the Fullprof, JANA 2006 and TOPAS software suites. The orthorhombic unit cell of $\gamma\text{-Na}_3\text{PS}_4$ was determined using Dicvol and the suitability of the face-centered space groups *Fddd* and *Fdd2* was determined by manual inspection of the systematic extinctions. Space group independent analysis of the scattering density using the charge-flipping algorithm Superflip indicated the absence of an inversion center, consistent with *Fdd2*. Nevertheless, the additional reflections of *Fdd2* compared to *Fddd* ($hko: h+k=4n$) were not observable, so the latter was chosen for further analysis.

Fourier synthesis of the observed diffraction intensities indicated strong electronic density around the 8a Wyckoff position ($1/8, 1/8, 1/8; 7/8, 7/8, 7/8$), consistent with a thenardite-like arrangement of PS_4^{3-} , analogous to those of SO_4^{2-} in the archetypical Na_2SO_4 ^{5,6}.

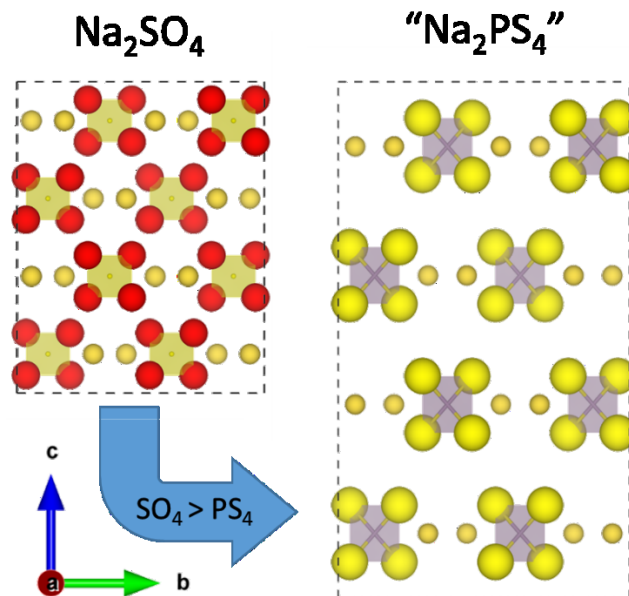


Figure S2. Relationship between the archetypical thenardite structure (Na_2SO_4) and that of $\gamma\text{-Na}_3\text{PS}_4$. Through expansion of the unit cell (mainly in the c -direction), and replacement of SO_4^{2-} with PS_4^{3-} , the anionic framework of $\gamma\text{-Na}_3\text{PS}_4$ is produced.

The above “ Na_2PS_4 ” thenardite structure is used as a starting model for Rietveld refinement of the structure and ab initio calculations as described below.

Rietveld refinement

Inspection of the diffraction data collected at 550°C reveal diffuse/delocalized scattering, atypical of classical crystalline solids. This is evident from the rapid diminution of Bragg peak intensities with increasing 2θ (i.e. scattering vector) and broad peaks of (electronic) scattering density upon Fourier transformation into real space. Typically, this is indicative of a strong degree of disorder and is modelled in Rietveld refinements using (an)isotropic displacement parameters (ADPs) and/or splitting atomic positions into multiple ones with partial occupation. In this framework, a multitude of approaches were used for the structural analysis of Na_3PS_4 ; involving different permutations of the above strategies for the different atoms with the goal of reaching a reasonable compromise between the number of fitted parameters and the quality of fit. The development of the approximate model presented here is a result of the following procedure:

- Based on the reflection intensities extracted from a Pawley fit, a charge flipping procedure was performed to identify the center of charge gravities of the P and S ions. Those were found at a distance of 1.99 \AA , which is close to the static bond distance of 2.05 \AA . This position and shape of the PS_4^{3-} unit was then maintained constant for the subsequent Rietveld refinements.
- The scattering density distribution around sulfur was modelled using a split site; i.e. two coincident partially occupied sulfur atoms. The positions were constrained to be identical, but ADPs were fitted separately in combination with a fractional occupancy constrained to stoichiometry (Figure S3a). This approach yielded a significantly better fit, compared to a single sulfur with anisotropic displacement parameters and utilizes less fitted parameters compared to models with multiple non-coincident sulfur atoms. For phosphorous, ADPs were similarly fitted

resulting in disk-like thermal motion. The obtained charge and positional distribution of the atoms of the PS_4^{3-} subunits is shown in Figure S3b. This was deemed necessary to capture the fact that the distortion of the PS_4^{3-} units are more complex than a simple vibrational behaviour, which could originate from the permanent redistribution of Na^+ ions around the tetrahedral unit (as also observed from MD simulations).

c. A simulated annealing approach was utilized to approximate the sodium distribution around the highly flexible PS_4^{3-} units. The distribution of Na was found to depend highly on the refined central position of sulfur. For that reason, empirically determined penalties for Na-S distances below 1.45 Å and for Na-P distances below 2 Å were applied in order to avoid tracking of sodium ions into the PS_4^{3-} polyhedra during the refinement (so called anti-bump criteria). These serve well to limit correlations arising from the unrestricted allocation of charge densities from small number of sodium ions around the PS_4^{3-} units. In this way, it was possible to derive a plausible Na^+ distribution based on 29 Na^+ ions on partially and equally occupied ($\approx 2.5\%$) general sites ($32h$) with identical isotropic temperature factors and the majority of Na-S distances significantly above 2 Å, as shown in Figure S3c.

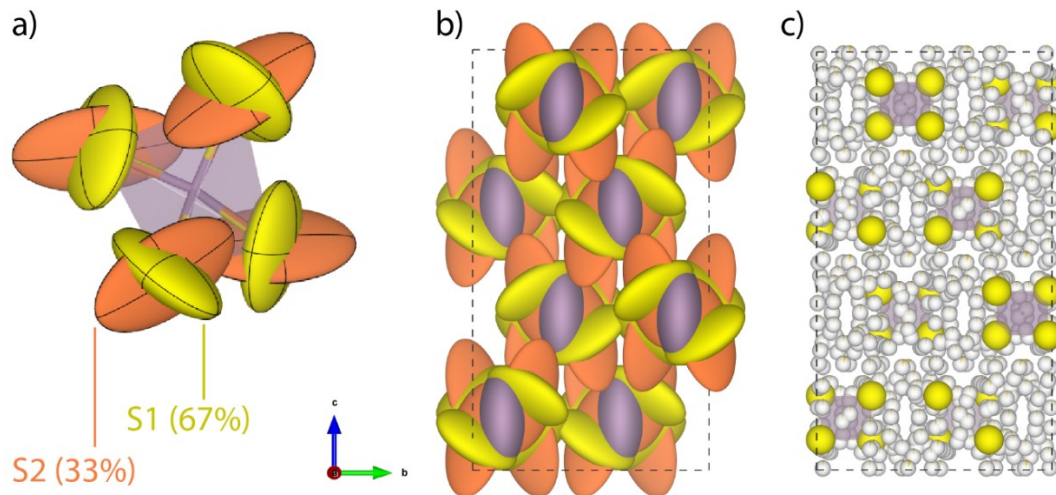


Figure S3. Visualisation of the structural model used in the Rietveld refinement of $\gamma\text{-Na}_3\text{PS}_4$. The PS_4^{3-} unit (a) is described by one phosphorous and two coinciding sulfur atoms all with independent ADPs. Ellipsoids shown with 10% probability in (a) and 50% in (b). The sodium ions are found to occupy most of the remaining volume not occupied by PS_4^{3-} (c).

Finally, all positions, displacement-, lattice- and peak shape parameters were simultaneously refined using the Rietveld method. The above model yields an excellent fit with the experimental data as shown in Figure S4, and the resulting structure is provided as a .cif file.

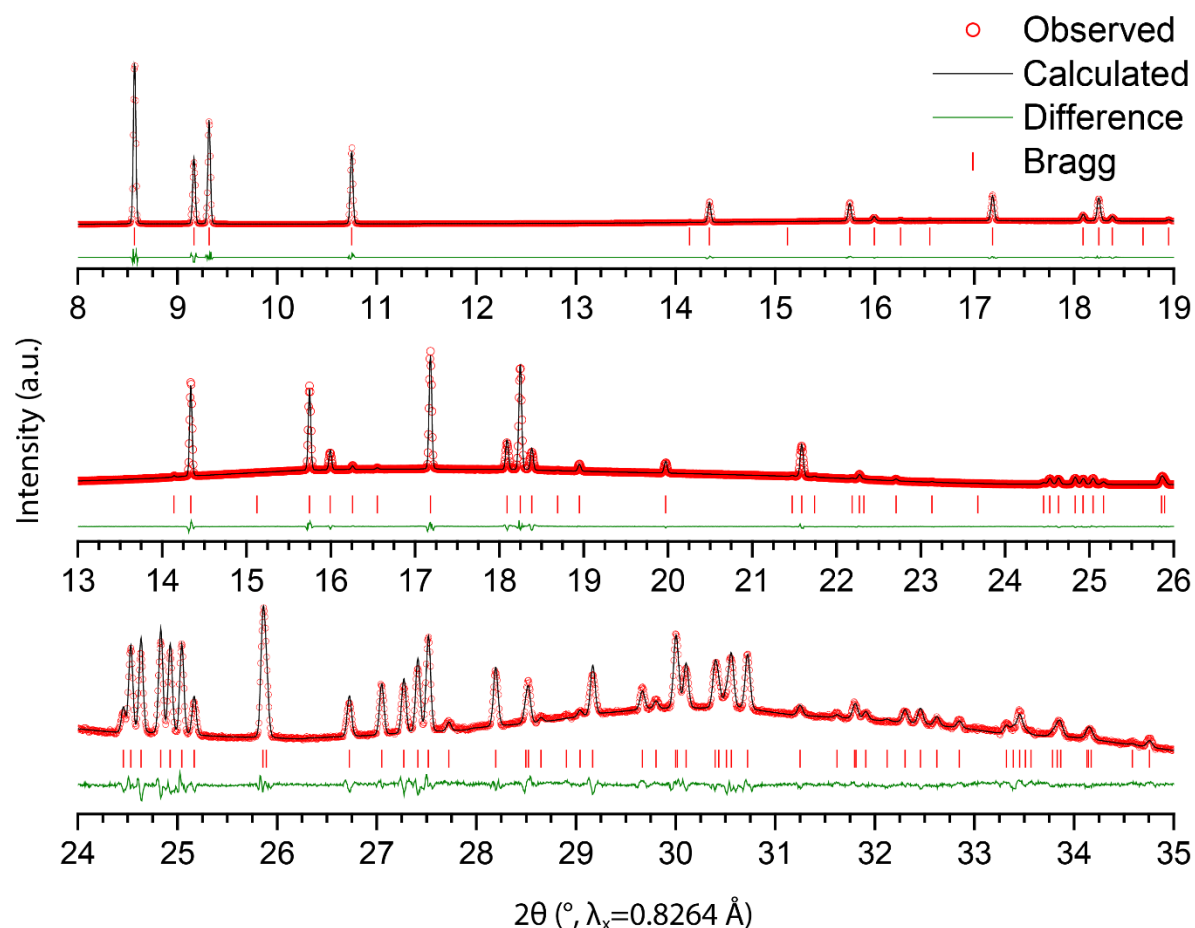


Figure S4. Rietveld refinement of the diffractogram of $\gamma\text{-Na}_3\text{PS}_4$. Three different angular ranges are shown, with the intensity scaled to the most intense reflection of this range for better visibility.

We note that the thermal parameters utilised to model the PS_4^{3-} unit are unusually large. This is consistent with the molecular dynamics simulations showing tremendous rotational and vibrational mobility. Given this mobility, the structural model which corresponds to the average structure needs to cover all possible conformations attainable leading to the large ADPs. We emphasize that this model is not free of correlation, and that the positions determined for the sodium ions can only be understood as an ensemble, which serves to approximate the electron density distribution of the sodium ions attesting to the strong delocalization of this sublattice. Finally, we note that given the limited contrast between the atomic form factors of Na, P, and S makes an unambiguous assignment of electronic density to specific species challenging.

Thermal analysis

Thermogravimetric analysis (TGA) and differential scanning calorimetry (DSC) measurements were performed simultaneously using a Netzsch Simultaneous thermal analyzer STA449F3 housed in an Ar-filled glovebox (Jacomex). The measurements were performed under flow of argon gas (60 ml/min) at a heating/cooling rate of 5 °C/min. Oxygen impurities in the argon gas were captured at temperatures of >300 °C by a metallic zirconium ring placed in-line before the sample.

Electrical characterization

Impedance spectroscopy was performed on samples pressed into pellets of 6 mm in diameter and approximately 3 mm in thickness. The pellets were placed in between 6-mm graphite paper electrodes (Papyex, Mersen) and mounted inside an HTSH-1100 sample holder (Bio-Logic) featuring Pt electrodes. Spectra were measured at multiple temperatures on heating from ambient to 600 °C controlled using a furnace (HTF-1100, Bio-Logic) by applying an AC excitation voltage of 50 mV from 10 Hz to 30 MHz using an MTZ-35 impedance analyzer (Bio-Logic). Conductivities were extracted by considering the observed real resistance and the geometry of the sample, which was assumed constant.

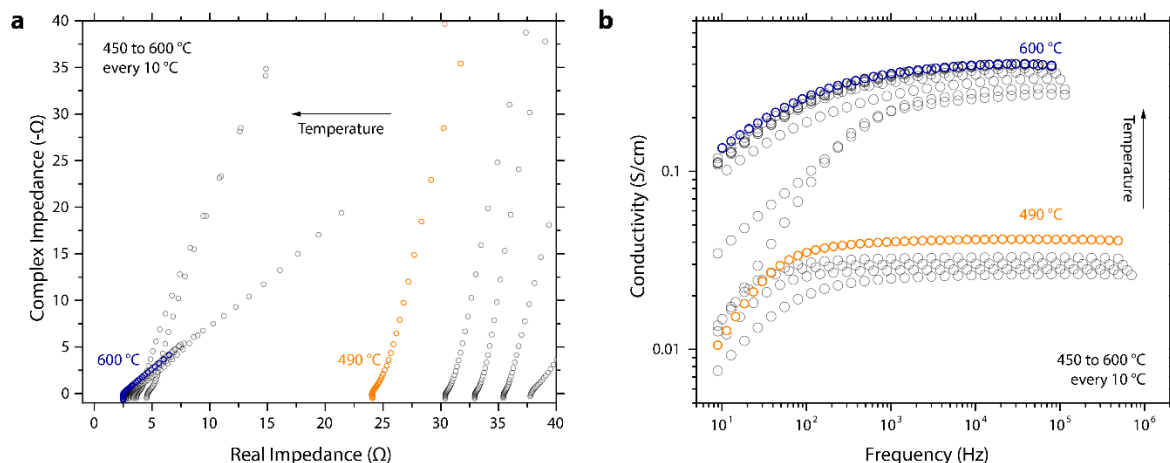


Figure S5. Evolution of impedance spectra for Na_3PS_4 in (a) Nyquist and (b) Bode-conductivity coordinates. Spectra shown for the temperature range 450-600 °C, every 10 °C. Highlighted are the spectra at 490 °C (orange) and 600 °C (blue). A monotonic decrease in resistance (increase in conductivity) is observed with a sharp discontinuity between 490 and 500 °C corresponding to the β -to- γ phase transition.

The activation energies at different temperature ranges were extracted by the typical modified Arrhenius relationship utilized for ionic conductors:

$$\sigma T = \sigma_0 e^{-E_a/kT}$$

where σ is the ionic conductivity, T is temperature, σ_0 is the Arrhenius prefactor, E_a is the activation energy and k is the Boltzmann constant.

We note that Na_3PS_4 becomes quite soft upon transition to the γ -polymorph and will plastically deform upon applied pressure. This is critical to consider when measuring impedance spectra as most setups rely on applied pressure to maintain electrical contact.

Quenching

Attempts have been made to stabilize the γ -polymorph at ambient temperature by means of quenching. Samples of α - Na_3PS_4 were sealed in SiO_2 tubes (10.5 mm diameter, 1.25 mm wall thickness), SiO_2 capillaries (1 mm diameter, 0.01 mm wall thickness) and steel tubes (10 mm diameter, 0.5 mm thickness) and heated to 550 °C. After maintaining the high temperature for 1 hr the samples were quickly quenched in ice-water. In all cases the β -polymorph is observed as the main resulting phase.

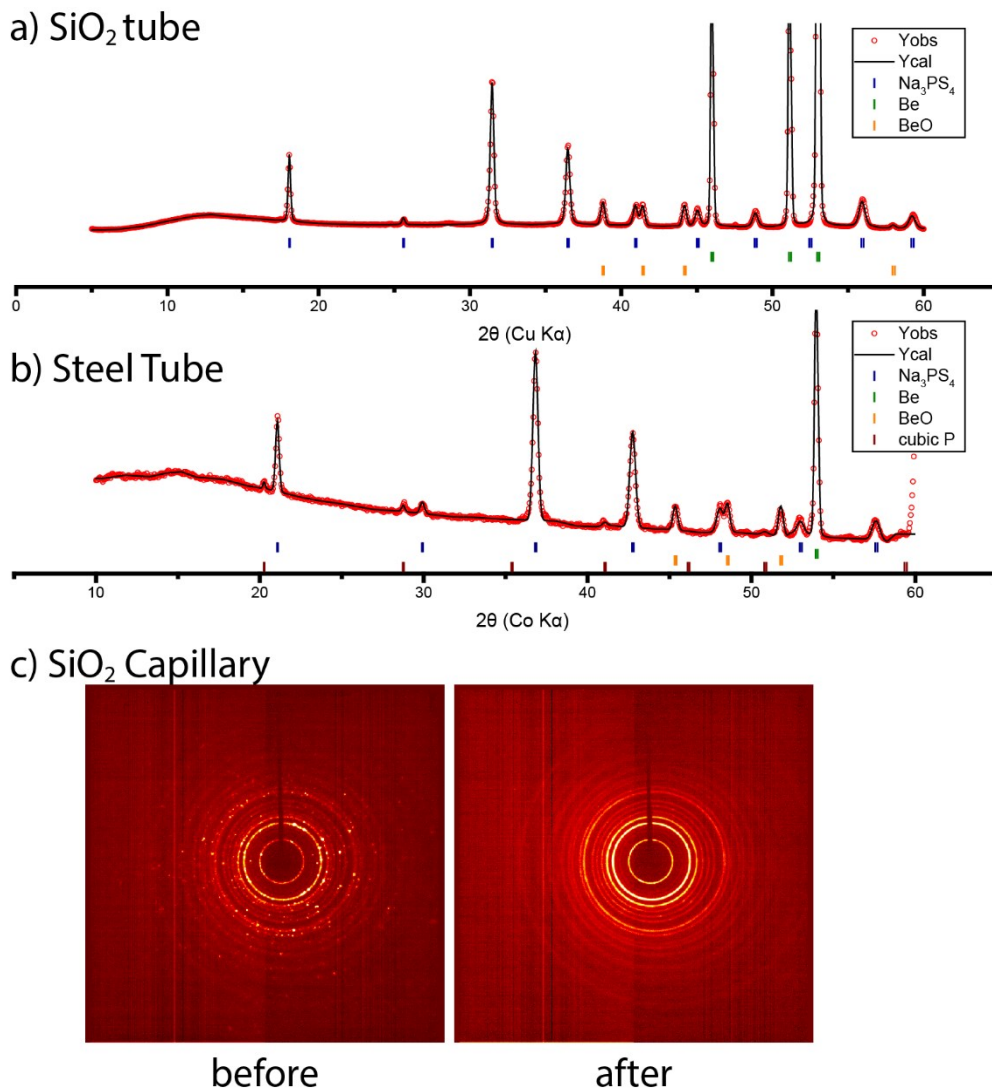


Figure S6. Diffractograms of Na_3PS_4 quenched from 550 °C. β - Na_3PS_4 is the main phase in all cases. Be and BeO peaks in (a) and (b) originate from the beryllium window used to protect samples from ambient exposure. An additional unidentified primitive cubic phase ($a=5.12$ Å) is observed in the sample quenched in steel (b) probably indicating reactivity with the quenching vessel. A distinct reduction of crystallite size is observed upon quenching in all cases and is especially obvious in the distinct Bragg spots turning to Debye rings in (c).

Ab initio Simulations

Calculations in this work were carried out using density functional theory (DFT) with the Vienna ab initio simulation package (VASP)⁷. Plane-wave cut-off energies of 520 and 400 eV were utilized for the geometry optimization and AIMD calculations, respectively. The projector augmented wave method⁸ and the PBEsol exchange-correlation functional⁹ were employed for all calculations. A k-point mesh spacing smaller than 0.05 \AA^{-1} was used for the geometry optimization calculations.

For the AIMD simulations, the k-space was sampled using the gamma-point only with a $3 \times 2 \times 1$ supercell containing 384 atoms. To aid Na-ion transport, Na vacancies were added to the supercell at a concentration of 5% with charge neutrality maintained by the addition of S vacancies, therefore giving a composition of $\text{Na}_{2.85}\text{PS}_{3.925}$. Statistical properties were obtained from >100 ps simulations using the NVT ensemble with a Nose–Hoover thermostat¹⁰. The AIMD calculations were carried out at 600, 750, 900 and 1050 K, with a time step of 2 fs. Self-diffusion data for Na were obtained from the mean square displacement (MSD) according to:

$$\langle r_i^2(t) \rangle = 6D_{\text{Na}}t$$

where $\langle r_i^2(t) \rangle$ is the MSD, D_{Na} is the diffusion coefficient for Na and t is time. Activation energies for Na^+ diffusion were extracted by fitting to an Arrhenius relationship of the form:

$$D_{\text{Na}} = D_0 e^{-E_a/kT}$$

where D_0 is the Arrhenius prefactor. Molecular dynamics were also performed without extrinsic vacancies at 900K (pristine Na_3PS_4) confirming the superionic nature of $\gamma\text{-Na}_3\text{PS}_4$ and only yielding a ~15% lower diffusion coefficient

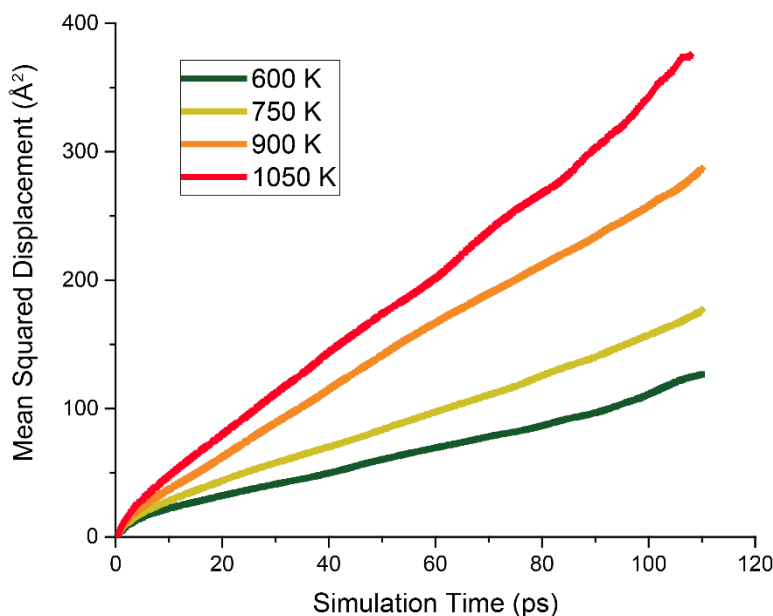


Figure S7. Mean-squared displacement (MSD) of Na atoms extracted from ab-initio molecular dynamics of $\gamma\text{-Na}_3\text{PS}_4$ showing the expected increase in Na^+ ion mobility with increasing temperature.

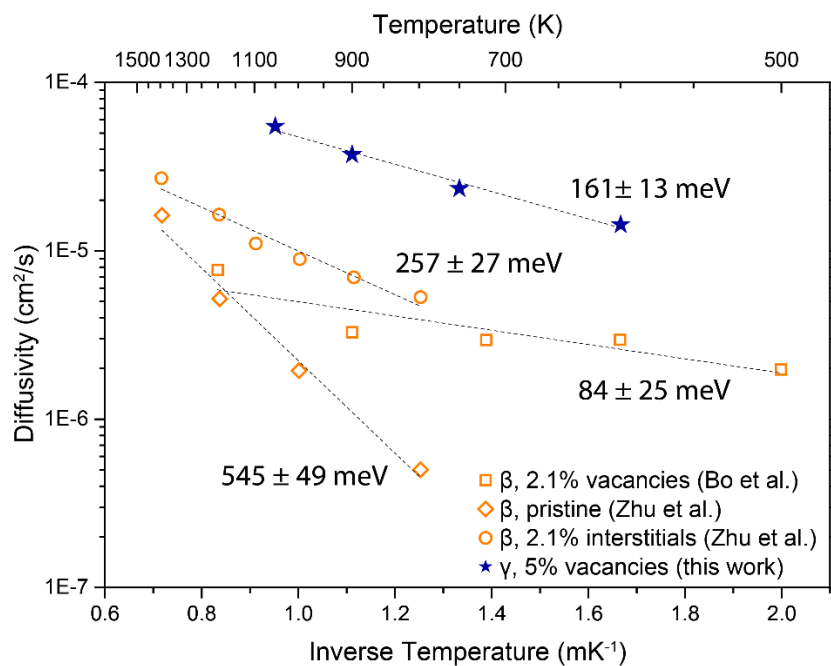


Figure S8. Diffusivity of Na⁺ from ab-initio molecular dynamics of Na₃PS₄. Literature data extracted from refs. ^{11,12}.

REFERENCES

- (1) Jansen, M.; Henseler, U. Synthesis, Structure Determination, and Ionic Conductivity of Sodium Tetrathiosphosphate. *J. Solid State Chem.* **1992**, *99*, 110–119. [https://doi.org/10.1016/0022-4596\(92\)90295-7](https://doi.org/10.1016/0022-4596(92)90295-7).
- (2) Krauskopf, T.; Culver, S. P.; Zeier, W. G. Local Tetragonal Structure of the Cubic Superionic Conductor Na_3PS_4 . *Inorg. Chem.* **2018**, *57*, 4739–4744. <https://doi.org/10.1021/acs.inorgchem.8b00458>.
- (3) Fauth, F.; Peral, I.; Popescu, C.; Knapp, M. The New Material Science Powder Diffraction Beamline at ALBA Synchrotron. *Powder Diffr.* **2013**, *28*, S360–S370. <https://doi.org/10.1017/S0885715613000900>.
- (4) Fauth, F.; Boer, R.; Gil-Ortiz, F.; Popescu, C.; Vallcorba, O.; Peral, I.; Fullà, D.; Benach, J.; Juanhuix, J. The Crystallography Stations at the Alba Synchrotron. *Eur. Phys. J. Plus* **2015**, *130*, 160. <https://doi.org/10.1140/epjp/i2015-15160-y>.
- (5) Zachariasen, W. H.; Ziegler, G. E. The Crystal Structure of Anhydrous Sodium Sulfate Na_2SO_4 . *Zeitschrift für Krist. - Cryst. Mater.* **1932**, *81*, 92–101. <https://doi.org/10.1524/zkri.1932.81.1.92>.
- (6) Nord, A. G. Refinement of the Crystal Structure of Thenardite, Na_2SO_4 (V). *Acta Chem. Scand.* **1973**, *27*, 814–822.
- (7) Kresse, G.; Furthmüller, J. Efficient Iterative Schemes for Ab Initio Total-Energy Calculations Using a Plane-Wave Basis Set. *Phys. Rev. B* **1996**, *54*, 11169–11186. <https://doi.org/10.1103/PhysRevB.54.11169>.
- (8) Blöchl, P. E. Projector Augmented-Wave Method. *Phys. Rev. B* **1994**, *50*, 17953–17979. <https://doi.org/10.1103/PhysRevB.50.17953>.
- (9) Perdew, J. P.; Ruzsinszky, A.; Csonka, G. I.; Vydrov, O. A.; Scuseria, G. E.; Constantin, L. A.; Zhou, X.; Burke, K. Restoring the Density-Gradient Expansion for Exchange in Solids and Surfaces. *Phys. Rev. Lett.* **2008**, *100*, 136406. <https://doi.org/10.1103/PhysRevLett.100.136406>.
- (10) Evans, D. J.; Holian, B. L. The Nose–Hoover Thermostat. *J. Chem. Phys.* **1985**, *83*, 4069–4074. <https://doi.org/10.1063/1.449071>.
- (11) Bo, S.-H.; Wang, Y.; Ceder, G. Structural and Na-Ion Conduction Characteristics of $\text{Na}_3\text{PS}_x\text{Se}_{4-x}$. *J. Mater. Chem. A* **2016**, *4*, 9044–9053. <https://doi.org/10.1039/C6TA03027K>.
- (12) Zhu, Z.; Chu, I.-H.; Deng, Z.; Ong, S. P. Role of Na^+ Interstitials and Dopants in Enhancing the Na^+ Conductivity of the Cubic Na_3PS_4 Superionic Conductor. *Chem. Mater.* **2015**, *27*, 8318–8325. <https://doi.org/10.1021/acs.chemmater.5b03656>.